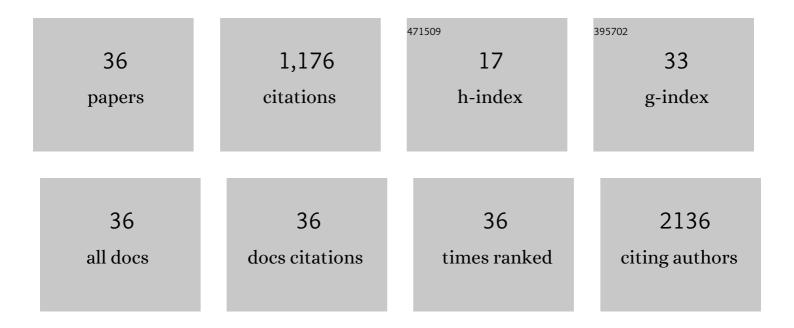
Erlend Hodneland

List of Publications by Year in descending order

Source: https://exaly.com/author-pdf/8535163/publications.pdf Version: 2024-02-01



EDIEND HODNELAND

#	Article	IF	CITATIONS
1	Fully Automatic Whole-Volume Tumor Segmentation in Cervical Cancer. Cancers, 2022, 14, 2372.	3.7	9
2	Wholeâ€Volume Tumor <scp>MRI</scp> Radiomics for Prognostic Modeling in Endometrial Cancer. Journal of Magnetic Resonance Imaging, 2021, 53, 928-937.	3.4	47
3	Automated segmentation of endometrial cancer on MR images using deep learning. Scientific Reports, 2021, 11, 179.	3.3	24
4	Well-Posedness and Discretization for a Class of Models for Mixed-Dimensional Problems with High-Dimensional Gap. SIAM Journal on Applied Mathematics, 2021, 81, 2218-2245.	1.8	3
5	A radiogenomics application for prognostic profiling of endometrial cancer. Communications Biology, 2021, 4, 1363.	4.4	14
6	A new framework for assessing subject-specific whole brain circulation and perfusion using MRI-based measurements and a multi-scale continuous flow model. PLoS Computational Biology, 2019, 15, e1007073.	3.2	24
7	Effect of temperature and concentration of impurities in the fluid stream on CO2 migration in the Utsira formation. International Journal of Greenhouse Gas Control, 2019, 83, 20-28.	4.6	13
8	<i>In Vivo</i> Detection of Chronic Kidney Disease Using Tissue Deformation Fields From Dynamic MR Imaging. IEEE Transactions on Biomedical Engineering, 2019, 66, 1779-1790.	4.2	17
9	Estimating the discretization dependent accuracy of perfusion in coupled capillary flow measurements. PLoS ONE, 2018, 13, e0200521.	2.5	9
10	Semi-automatic 3D morphological reconstruction of neurons with densely branching morphology: Application to retinal All amacrine cells imaged with multi-photon excitation microscopy. Journal of Neuroscience Methods, 2017, 279, 101-118.	2.5	6
11	Workflow sensitivity of post-processing methods in renal DCE-MRI. Magnetic Resonance Imaging, 2017, 42, 60-68.	1.8	7
12	A practical guideline for <i>T</i> ₁ reconstruction from various flip angles in MRI. Journal of Algorithms and Computational Technology, 2016, 10, 213-223.	0.7	5
13	Quantification of Single-Kidney Function and Volume in Living Kidney Donors Using Dynamic Contrast-Enhanced MRI. American Journal of Roentgenology, 2016, 207, 1022-1030.	2.2	14
14	Physical Models for Simulation and Reconstruction of Human Tissue Deformation Fields in Dynamic MRI. IEEE Transactions on Biomedical Engineering, 2016, 63, 2200-2210.	4.2	10
15	Fractional anisotropy shows differential reduction in frontal-subcortical fiber bundlesââ,¬â€A longitudinal MRI study of 76 middle-aged and older adults. Frontiers in Aging Neuroscience, 2015, 7, 81.	3.4	14
16	Use of 3D DCE-MRI for the Estimation of Renal Perfusion and Glomerular Filtration Rate: An Intrasubject Comparison of FLASH and KWIC With a Comprehensive Framework for Evaluation. American Journal of Roentgenology, 2015, 204, W273-W281.	2.2	25
17	Melanoma brain metastasis is independent of lactate dehydrogenase A expression. Neuro-Oncology, 2015, 17, 1374-1385.	1.2	10
18	Intercellular transfer of transferrin receptor by a contactâ€; Rab8â€dependent mechanism involving tunneling nanotubes. FASEB Journal, 2015, 29, 4695-4712.	0.5	46

Erlend Hodneland

#	Article	IF	CITATIONS
19	Quantitative lung ventilation using Fourier decomposition MRI; comparison and initial study. Magnetic Resonance Materials in Physics, Biology, and Medicine, 2014, 27, 467-476.	2.0	26
20	Segmentation-Driven Image Registration-Application to 4D DCE-MRI Recordings of the Moving Kidneys. IEEE Transactions on Image Processing, 2014, 23, 2392-2404.	9.8	27
21	Normalized gradient fields for nonlinear motion correction of DCE-MRI time series. Computerized Medical Imaging and Graphics, 2014, 38, 202-210.	5.8	31
22	Registration of FA and T1-Weighted MRI Data of Healthy Human Brain Based on Template Matching and Normalized Cross-Correlation. Journal of Digital Imaging, 2013, 26, 774-785.	2.9	25
23	Automated Tracking of Nanoparticle-labeled Melanoma Cells Improves the Predictive Power of a Brain Metastasis Model. Cancer Research, 2013, 73, 2445-2456.	0.9	49
24	White matter fiber tracking directed by interpolating splines and a methodological framework for evaluation. Frontiers in Neuroinformatics, 2013, 7, 13.	2.5	2
25	Rab3D Is Critical for Secretory Granule Maturation in PC12 Cells. PLoS ONE, 2013, 8, e57321.	2.5	18
26	Episodic memory of APOE ε4 carriers is correlated with fractional anisotropy, but not cortical thickness, in the medial temporal lobe. NeuroImage, 2012, 63, 507-516.	4.2	19
27	Automated approaches for analysis of multimodal MRI acquisitions in a study of cognitive aging. Computer Methods and Programs in Biomedicine, 2012, 106, 328-341.	4.7	17
28	Cortico-striatal connectivity and cognition in normal aging: A combined DTI and resting state fMRI study. NeuroImage, 2011, 55, 24-31.	4.2	135
29	Distinct Roles of Myosin Va in Membrane Remodeling and Exocytosis of Secretory Granules. Traffic, 2010, 11, 637-650.	2.7	20
30	A Unified Framework for Automated 3-D Segmentation of Surface-Stained Living Cells and a Comprehensive Segmentation Evaluation. IEEE Transactions on Medical Imaging, 2009, 28, 720-738.	8.9	29
31	Selective block of tunneling nanotube (TNT) formation inhibits intercellular organelle transfer between PC12 cells. FEBS Letters, 2009, 583, 1481-1488.	2.8	179
32	Four-Color Theorem and Level Set Methods for Watershed Segmentation. International Journal of Computer Vision, 2009, 82, 264-283.	15.6	27
33	In thrombin stimulated human platelets Citalopram, Promethazine, Risperidone, and Ziprasidone, but not Diazepam, may exert their pharmacological effects also through intercalation in membrane phospholipids in a receptor-independent manner. Journal of Chemical Biology, 2009, 2, 89-103.	2.2	15
34	Tunneling nanotube (TNT)-like structures facilitate a constitutive, actomyosin-dependent exchange of endocytic organelles between normal rat kidney cells. Experimental Cell Research, 2008, 314, 3669-3683.	2.6	126
35	A simple method to calculate the accessible volume of protein-bound ligands: Application for ligand selectivity. Journal of Molecular Graphics and Modelling, 2007, 26, 429-433.	2.4	1
36	Epac1 and cAMP-dependent Protein Kinase Holoenzyme Have Similar cAMP Affinity, but Their cAMP Domains Have Distinct Structural Features and Cyclic Nucleotide Recognition. Journal of Biological Chemistry, 2006, 281, 21500-21511.	3.4	133